

Experimental and numerical studies on the cyclic behavior of R/C hollow bridge piers with corroded rebars

D. Cardone^{*}, G. Perrone and S. Sofia

Scuola di Ingegneria, Università degli Studi della Basilicata, Via dell'Ateneo Lucano 10, 85100, Potenza, Italy

(Received November 8, 2011, Revised February 16, 2012, Accepted February 20, 2012)

Abstract. A comprehensive experimental program of cyclic tests on 1:3-scale models of bridge piers is going to be carried out at the Laboratory of Structures and Materials of the University of Basilicata. The testing models include eight RC single shaft piers with hollow circular cross section. Four piers have been realised using corroded steel rebars. In this paper, the results of preliminary numerical simulation analyses of the cyclic behaviour of the piers, carried out with Opensees using fiber-based models, are presented. Pull-out and lap-splice effects of steel rebars have been taken into account in the numerical analyses. First, the experimental specimens and the test set up are presented. Next, the results of the numerical analyses are discussed. In the numerical analyses, different configurations and levels of corrosion have been considered. The effective stiffness and equivalent damping of the piers is reported as a function of pier ductility and pier drift.

Keywords: RC piers; nonlinear cyclic behavior; numerical simulation analyses; corrosion of steel rebars.

1. Introduction

The seismic assessment of existing bridges is a primary concern, especially in regions where most bridges have been designed and built without specific rules and details for earthquake resistant structures. Past seismic events have shown that sub-standard details results in extensive damage or collapse during strong earthquakes, with dramatic consequences in terms of economic and social costs.

The Italian highway network consists of approximately 5000 Reinforced Concrete (RC) bridges, most of them designed in the '60 and '70 considering gravity loads only or according to old seismic codes, based on elastic design approaches. The seismic vulnerability of many existing Italian highway bridges is then expected to be very high.

An extensive program of experimental tests is going to be carried out at the Laboratory of Structures and Materials of the University of Basilicata, in order to assess the seismic behaviour of typical pier-deck sub-systems. The experimental program consists of a series of cyclic tests on eight 1:3-scale pier-deck sub-systems characterized by single shaft RC piers with hollow circular

^{*}Corresponding author, Professor, E-mail: donatello.cardone@unibas.it

cross section and two different effective heights. Four piers have been realized using corroded rebars accomplished with an accelerated corrosion process, whose characteristics have been determined based on a preliminary evaluation of deterioration mechanisms for aging bridge piers. The experimental tests will be performed considering at least two different pier-deck connections, i.e., (1) fixed steel connections and (2) semi-rigid neoprene connections.

So far, a number of experimental tests have been performed to investigate the nonlinear cyclic behavior of RC bridge piers.

The first studies on the flexural strength and ductility of RC columns with circular hollow section, characterized by two layers of longitudinal and transverse reinforcement, have been conducted by Whittaker *et al.* (1987), which pointed out that the core of the RC columns was well confined by the double layer of reinforcement and the columns performed in a ductile manner during cyclic lateral loading.

Zahn *et al.* (1990) investigated the flexural strength and ductility of RC circular hollow columns characterized by one layer of longitudinal reinforcement only and transverse reinforcement realized with a spiral placed on the outer face of the section. Results have shown that all columns collapsed due to concrete crushing in the compression zone of the section. No signs of shear failure have been observed in any of the tests.

Ranzo and Priestley (2001) conducted some cyclic tests on three large size specimens, characterized by one layer of longitudinal reinforcement only and transverse reinforcement realized with a spiral placed on the outer face of the section. The results indicated that the implosion of concrete in the inner surface, under the effect of high bending and shear forces, governs the activation of the strength degradation mechanism. For the same shear strength, pier models with higher flexural capacity were found to require thicker walls in order to prevent concrete spalling in the inside wall surface.

Cyclic tests on three different bridge piers with hollow circular cross section and different layout of steel lateral reinforcement have been performed by Yeh *et al.* (2001), to study the flexure-shear interaction. Results have shown that, when the ultimate capacity of the pier is dominated by bending moment, collapse occurs due to failure in tension of some longitudinal steel bars at the bottom of the column after buckling during previous compression cycles. On the contrary, when the ultimate capacity of the pier is determined by a bond failure of spliced longitudinal reinforcing bars in the plastic hinge region, fewer and wider cracks occur; the plastic hinge do not fully develop and much lower displacement ductility is observed. Finally, when the ultimate capacity of the pier is dominated by shear, concrete crushing at the bottom of the specimen followed by failure in tension of some longitudinal bars occurs; the plastic hinge do not fully develop and very low displacement ductility is observed.

Further experimental studies, based on cyclic loading tests, on RC bridge columns with rectangular hollow cross section, designed without seismic details, have been performed by Kim *et al.* (2000), Yeh (2002) and Pinto (2003).

More recently, experimental and numerical studies on the cyclic behaviour of RC hollow bridge piers have been also conducted by Calvi *et al.* (2005), which considered ten 1:4-scale pier models with square cross section with side of 450 mm and thickness of 75 mm. Two different pier heights (900 mm and 1850 mm, respectively) and four different axial load ratios, ranging from 0.06 to 0.21, have been considered in the tests. Poor confinement, inadequate shear strength, insufficient overlap length have been examined in the tests. Comparisons with the results of numerical simulation analyses have shown that fibre models, while being quite good in capturing the flexural response of slender RC hollow piers, must be corrected in order to predict correctly the

shear-flexural response of short piers, by including a sort of stiffness reduction due to shear cracking.

A number of numerical studies on the cyclic behavior of core-hollow bridge piers have been also performed in the last decade. Kang *et al.* (2000), Liu and Foster (2000) and Kwon and Spacone (2002) carried out numerical simulation analyses of the cyclic behavior of RC piers considering different modelling approaches for reinforced concrete (Sadrnejad *et al.* 2006).

A fracture-plastic model (Červenka and Papanikolaou 2008) has been also proposed and applied for the numerical simulation analysis of the cyclic behaviour of RC hollow cross section piers in a recent work by Papanikolaou and Kappos (2009a, 2009b), which examined issues related with concrete confinement in RC hollow cross section piers. The authors conclude that three-dimensional analysis can be established as a promising alternative to empirical confinement models because it is unrestricted in terms of section geometry and reinforcement arrangement complexities. It can be also considered as a cost-effective counterpart to experimental testing for the assessment or design of RC bridge piers.

The results of refined numerical simulation analyses of the cyclic behaviour of RC hollow cross section piers, based on a 3D solid finite element mesh using a continuum damage model (Faria *et al.* 1998), have been recently presented by Delgado *et al.* (2011). The results of the numerical simulation analyses have been compared with experimental results. The comparison between numerical and experimental results highlighted the adequacy of the modelling strategy adopted, particularly for shear effects and concrete behaviour under high shear forces. Only the energy dissipation capacity of the piers was not always adequately simulated because of the difficulty in reproducing crack closing phenomena.

In this paper, the results of accurate numerical simulation analyses, carried out with the finite element program OPENSEES (McKenna *et al.* 2000), are presented. The main scope of the numerical simulation analyses was that of defining the displacement time histories to be applied in the forthcoming experimental cyclic tests. From this point of view, the numerical simulation analyses under consideration can be considered as a “blind test” of the cyclic behaviour of R/C piers with and without corroded rebars.

In the numerical analyses, piers have been modelled using fiber elements, with reasonable computational efforts, in accordance with the aim of the simulation analyses that is to design the forthcoming experimental program. The constitutive laws of materials have been calibrated based on the results of the characterization tests on concrete specimens, pure and corroded steel rebars. Finally, different configurations and levels of corrosion have been considered, in order to evaluate the influence of corrosion on the cyclic behaviour of the piers. The effects of pull-out and lap-splice of steel rebars have been also examined.

2. Deterioration mechanisms for aging bridge piers

Bridges are often threatened by the ill effects of aging and deterioration due harsh environmental conditions. According to recent studies (Gosh and Padgett 2012), the evaluation of seismic vulnerability of highway bridges should also take into account the time evolving loss of structural capacity because an aging bridge is naturally expected to be more vulnerable to seismic ground motions.

Among all the sources of deterioration and aging, special attention deserves the corrosion mechanisms of reinforcing steel bars embedded in concrete. Generally, this phenomenon can be

ascribed to the prolonged exposure of R/C piers to chlorides from two main sources: deicing salt and marine environment.

For both deicing and marine exposure, the corrosion mechanism of reinforcing steel bars embedded in concrete can be represented by the Fick's second law of diffusion through a semi-infinite solid (Stewart and Rosowsky 1998). First, however, the concentration of chloride ions in concrete must reach a critical threshold to dissolve the protective passive film around the reinforcement. Next, the corrosion initiation time is found to typically depend on the environmental exposure condition.

For deicing salt exposure, the corrosion initiation time can be evaluated with the relationship derived by Thoft-Christensen *et al.* (1998)

$$T_{i,deicing} = \frac{x^2}{4D_c} \left[\operatorname{erf}^{-1} \left(\frac{C_0 - C_{cr}}{C_0} \right) \right]^{-2} \quad (1)$$

where, $T_{i,deicing}$ is the corrosion initiation time due to deicing salt exposure, x is the concrete cover, D_c is the diffusion coefficient, C_0 is the equilibrium chloride concentration at the concrete surface, C_{cr} is the critical chloride concentration that causes dissolution of the protective passive film around the reinforcement and initiates corrosion and erf is the Gaussian error function.

Corrosion initiation time for RC members in marine environment can be estimated based on the relationship proposed by Choe *et al.* (2009)

$$T_{i,marine} = \left[\frac{x R_{cl,0}}{4 K_c K_e (t_0)^{cl}} \left\{ \operatorname{erf}^{-1} \left(1 - \frac{C_{cr}}{C_0} \right) \right\}^{-2} \right]^{\frac{1}{(1-n_{cl})}} \quad (2)$$

where, $R_{cl,0}$ is the chloride penetration resistance (inverse of diffusion coefficient) determined from compliance tests, K_c is the curing factor, K_e is the environmental factor, t_0 is the age of concrete when the compliance test is performed, n_{cl} is the age exponent that incorporates the densification of cement paste due to further hydration (Choe *et al.* 2009).

Once corrosion initiates by either chloride exposure from deicing salts or marine exposure, the time dependent loss of reinforcement cross-sectional area, $A(t)$, can be expressed as (Thoft-Christensen *et al.* 1998)

$$A(t) = \begin{cases} nD_i^2 \frac{\pi}{4} & \text{for } t \leq T_i \\ n(D(t))^2 \frac{\pi}{4} & \text{for } T_i \leq t \leq T_i + D_i / r_{corr} \\ 0 & \text{for } t \geq T_i + D_i / r_{corr} \end{cases} \quad (3)$$

where, n is the number of reinforcement bars, D_i is the initial diameter of steel reinforcement, t is the elapsed time in years, r_{corr} is the rate of corrosion and $D(t)$ is the reinforcement diameter at the end of $(t - T_i)$ years, which can be expressed as

$$D(t) = D_i - r_{corr} (t - T_i) \quad (4)$$

In this paper, reference to R/C piers with concrete cover contaminated by chlorides, located in ambient exposed to salt deicing, with relative humidity of 90-95%, has been made. In these conditions, a corrosion rate (r_{corr}) of the order of 0.2 mm/year can be assumed (Bertolini *et al.* 2004). A corrosion initiation time of approximately 5 years has been derived from Eq. (1), assuming $x = 30$ mm, $D_c = 1.29$ cm²/year, $C_0 = 0.1$ wt % concrete and $C_{cr} = 0.04$ wt % concrete, in accordance with Gosh and Padgett (2012).

Two levels of corrosion, represented by a reduction of diameter of the steel bars of 15% and 30%, respectively, have been then considered. Based on Eq. (4), they correspond to an exposure time in moderate-to-high harsh environmental conditions of the order of 20 years and 40 years, respectively, including the corrosion initiation time of approximately 5 years.

In the fiber finite element model, the deterioration phenomena have been captured through a reduction of cross-section area of the longitudinal reinforcement bars and a loss of bond strength between steel and concrete. In accordance with the results of the parametric study conducted by (Gosh and Padgett 2012), other potential secondary effects such as: (1) cracking and spalling of cover concrete, loss of confinement effectiveness due to corrosion of steel ties, etc., have been neglected, they have a relatively small effect on the seismic resistance of R/C piers with low shear reinforcement ratios.

Concerning bond strength, experimental pull-out tests, carried out by Auyeung *et al.* (2000) on corroded reinforcement steel bars, have shown that, when the loss of mass exceeds 2%, the bond strength of corroded steel bars considerably decreases, tending with exponential law to the bond strength typical of smooth steel bars. As a consequence, in this study, reference to the bond law proposed by the model code CEB-FIP (CEB 1993) for smooth reinforcing steel rebars has been made, to account for the deterioration of the bond strength induced by corrosion.

3. Experimental models

3.1 Test specimens

The experimental models include eight 1:3-scale RC single shaft piers (see Fig. 1) with hollow circular cross section, with external diameter of 1 m (corresponding to 3 m in the full-scale prototype) and thickness of 125 mm (corresponding to 375 mm the full-scale prototype). Four pier models have effective height of 3.3 m (i.e., 10 m in the full-scale prototype) while the other four present effective height of 1.70 m (i.e., 5 m in the full-scale prototype). The geometric and mechanical characteristics of the pier models (i.e., pier type and dimensions, steel reinforcement ratios, material characteristics, vertical loads transmitted by the deck, etc.) have been derived from the examination of the piers of several multispan simply-supported deck bridges of the A16 (Napoli-Canosa) Italian highway, characterized by single shaft RC piers with hollow circular cross section and effective height ranging from 6 m to 12 m.

The piers have been realised using micro-concrete, due to the reduced dimensions of the pier models. Two concrete mixes with Portland cement (type II/AL), aggregates (sand) with grain size lower than 5 mm and water/cement ratio equal to 0.55 (mix A) and 0.85 (mix B) were prepared. A superfluidifier (Superflux 2003 – AXIM Italia) in the amount of 1.5% the weight of cement was added to the mix.

The pier models have been equipped with a stiff foundation and a pier cap (see Fig. 1), both realised with C30/35 standard concrete. B450C steel has been used for steel reinforcement.

The steel reinforcement of the tall piers consists of 20 8 mm diameter longitudinal bars, equally spaced along the inner and outer curved surface of the pier (see Fig. 2(a)). The short piers present 48 8 mm diameter longitudinal bars, equally spaced along the inner and outer curved surface of the pier (see Fig. 2(b)). The transverse reinforcement of both tall and short piers consists of 4 mm diameter stirrups at 10 cm step. Corroded longitudinal steel reinforcement has been used for two tall piers and two short piers. The corrosion of steel rebars has been accomplished with an accelerated corrosion process (see next section). In this regard, it is worth noting that the level of corrosion considered for the experimental models (represented by a reduction of approximately 15% of the diameter of the steel bars), corresponds to a natural corrosion process, due to deicing salt exposure, of approximately 20 years. Obviously, this time is not compatible with any experimental program. Basically, that's why an accelerated corrosion process of individual steel bars has been performed. As a matter of fact, the only possible alternative would be to apply the accelerated corrosion process to individual steel bars previously embedded in a thin core of concrete (external diameter less than 25 mm, to be compatible with the cover concrete of the experimental models). Most probably, this would not have changed the final result (i.e., the morphology and properties of the corroded steel bars), assuming the same initial target (15% reduction of the bar diameter).

In the following, the piers are identified by three labels (see Fig. 1). The first label refers to the height of the pier (T: tall, SH: short). The second label refers to the concrete mix (A: mix type A, B: mix type B). The third label refers to the type of longitudinal reinforcement (C: corroded, NC: not corroded).



Fig. 1 Experimental models: Tall (T) and Short (SH) piers, Corroded (C) and not corroded (NC) reinforcement, type A and type B of micro concrete

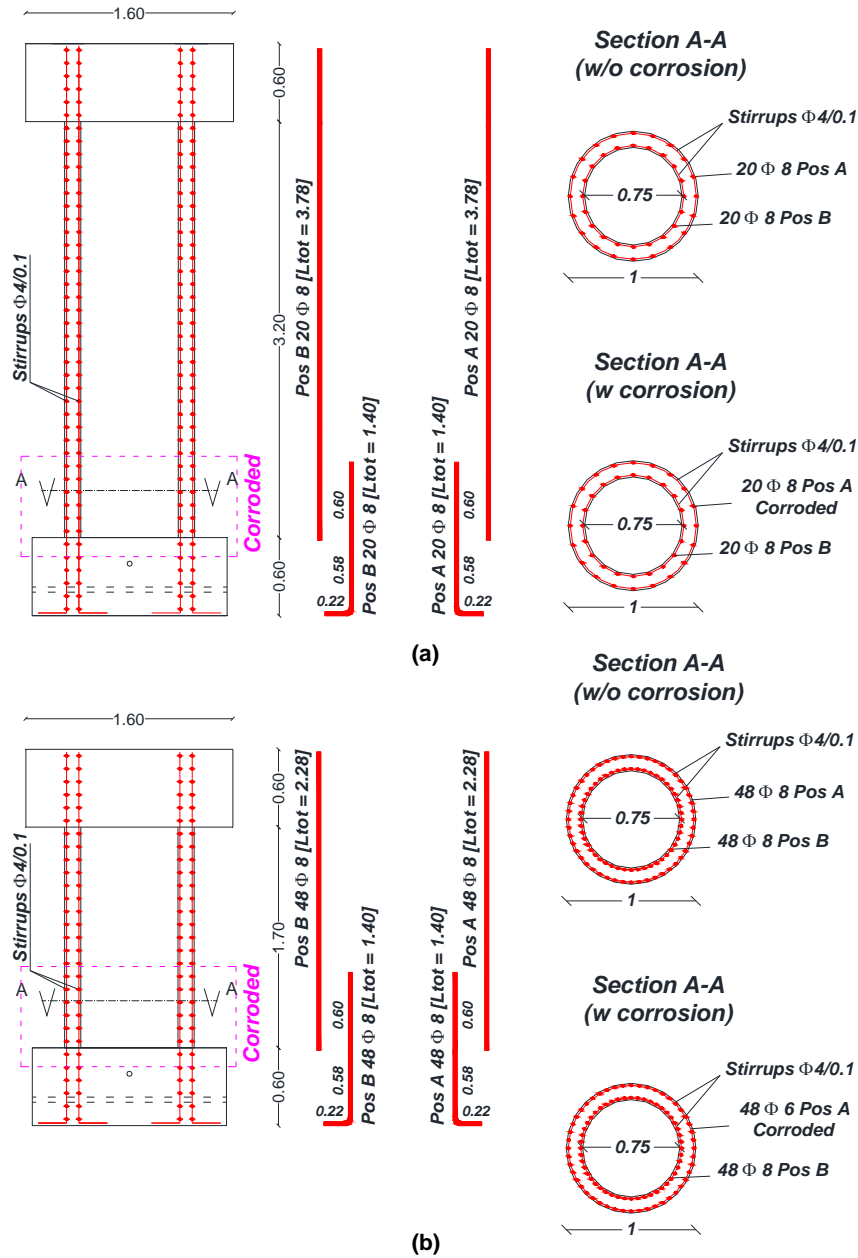


Fig. 2 Layout of pier reinforcement for: (a) Tall and (b) Short piers

3.2 Artificial corrosion of steel rebars

The artificial accelerated corrosion process has been realised through the passage of electricity in an electrical circuit composed by an AC/DC converter connected to a steel rebar, partially immersed in a 3% salt-water solution, and a copper bar (see Fig. 3). To save time, 21 steel bars have been corroded simultaneously, by realising a series of circuits as shown in Fig. 3.

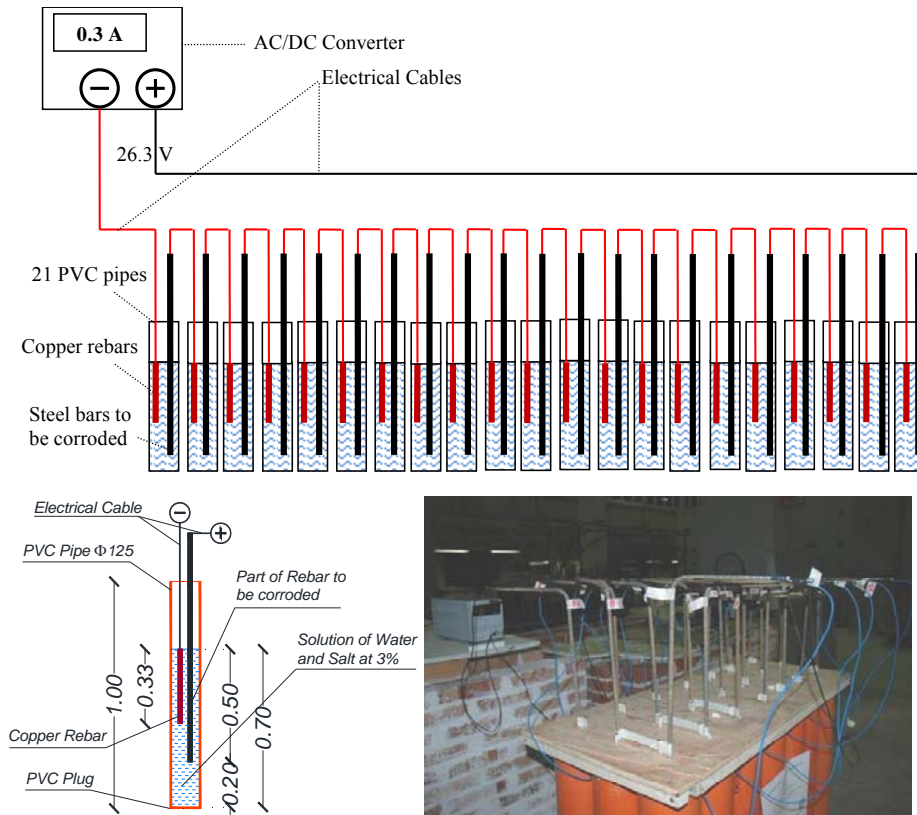


Fig. 3 Accelerated corrosion process set-up

The accelerated corrosion process was calibrated to achieve a 15% reduction of the diameter of the steel bar, corresponding to an elapsed time, after corrosion initiation (see Eq. (1)), of approximately 15 years in moderate-to-high aggressive environmental conditions, according to Eq. (4). The current intensity and duration of the process has been defined based on the Faraday's law

$$\Delta m = \frac{t \cdot A \cdot I}{Z \cdot F} \quad (6)$$

where t is the duration of the process, A is the atomic weight of iron (58.85 g/mol), I is the current intensity, Z is the valence taken equal to 2 and F is the Faraday's constant equal to 96.487 C/mol. Approximately 10 days, with current at 0.3 Amp, occurred to achieve the target reduction of the bar diameter. The corrosion has been applied to both pier bars and corresponding foundation bars, for a length of 500 mm, at the extremity of each bar (see Fig. 2(a)). The corrosion was intentionally concentrated in the critical zone of the pier, where plastic deformations are expected to occur under strong earthquakes.

The corrosion process not only produced a diameter reduction of the rebar but also a significant change in the mechanical characteristics of steel, particularly of its yield stress and ductility (see next section for details).

3.3 Materials characterization

The mechanical behaviour of steel and micro-concrete has been evaluated by experimental tests on specimens taken during the construction of the pier models. In particular, twenty 150x150x150 mm cubic specimens and eight 120 mm diameter by 240 mm height cylindrical specimens have been cast and tested after 28 days. The cubic specimens have been subjected to standard failure tests in compression, while the cylindrical specimens to loading-unloading cyclic tests in compression.

The failure tests on cubic specimens pointed out an average concrete strength of 30.75 MPa for mix A and 19.7 MPa for mix B.

The sensor set up in the loading-unloading tests consisted in one load cell, two inductive displacement transducers, connecting the steel plates of the press, and three potentiometric extensimeters, equally spaced at 120 degrees in the middle of the specimen (see Fig. 4(a)).

The stress-strain relationships derived from the loading-unloading compression tests on cylindrical specimens (see Fig. 4(b)), properly adjusted to account for the results of the failure tests on the cubic specimens, have been used to calibrate the constitutive law of concrete for numerical analysis. In Table 1 the main mechanical characteristics of micro-concrete (mix type A and type B) are summarised. They include: (1) initial Young modulus, (2) peak strength, (3) strain corresponding to the peak strength, (4) average loading-unloading stiffness, (5) residual stress and (6) ultimate strain.

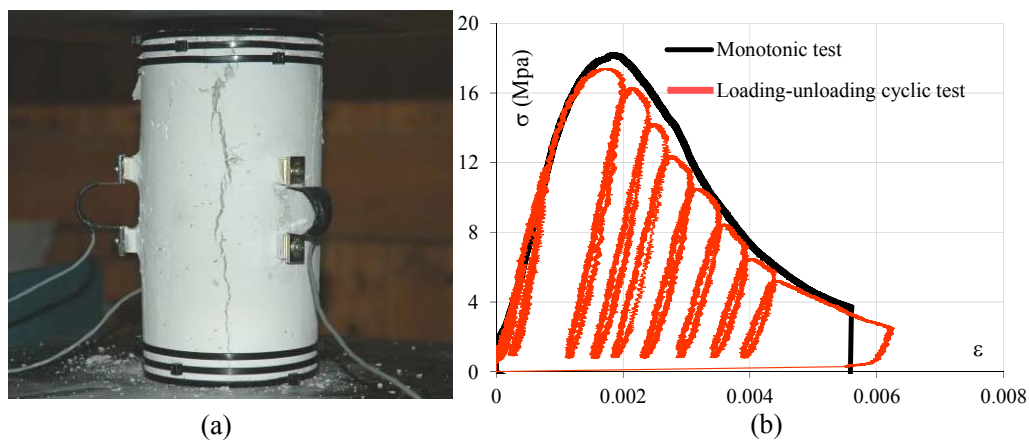


Fig. 4 (a) Sensor set-up for compression tests on cylindrical concrete specimens and (b) Typical results of monotonic and loading-unloading cyclic tests (mix type B specimens)

Table 1 Main mechanical characteristics of the mix A and mix B of micro-concrete

| | E (MPa) | f_c (MPa) | ϵ_c (%) | K_{lu} (MPa) | f_r (MPa) | ϵ_r (%) |
|----------------|-----------|-------------|------------------|----------------|-------------|------------------|
| MIX - A | 21720 | 28.0 | 0.169 | 16875 | 3.0 | 0.45 |
| MIX - B | 17239 | 17.6 | 0.178 | 13365 | 3.0 | 0.55 |

The mechanical behaviour of steel has been determined through failure tests in tension, carried out on both corroded and not corroded samples of steel bars (Fig. 5(a)). During the tests, the strain of the samples has been monitored by means of an extensimeter with 20 mm stroke, put in the middle of the specimen. In Fig. 5(b) the typical stress-strain relationships obtained for corroded and not corroded samples are compared. As expected, the artificial corrosion process produced a reduction of the bar diameter of the order of 15%, however, it also determined appreciable changes in the stress-strain behaviour of steel. In the case under consideration, for instance, the yield and ultimate strengths of steel turn out to be decreased approximately by 20%, due to corrosion. At the same time, the ultimate strain turns out to be reduced by approximately 30% and the yield plateau practically disappears.

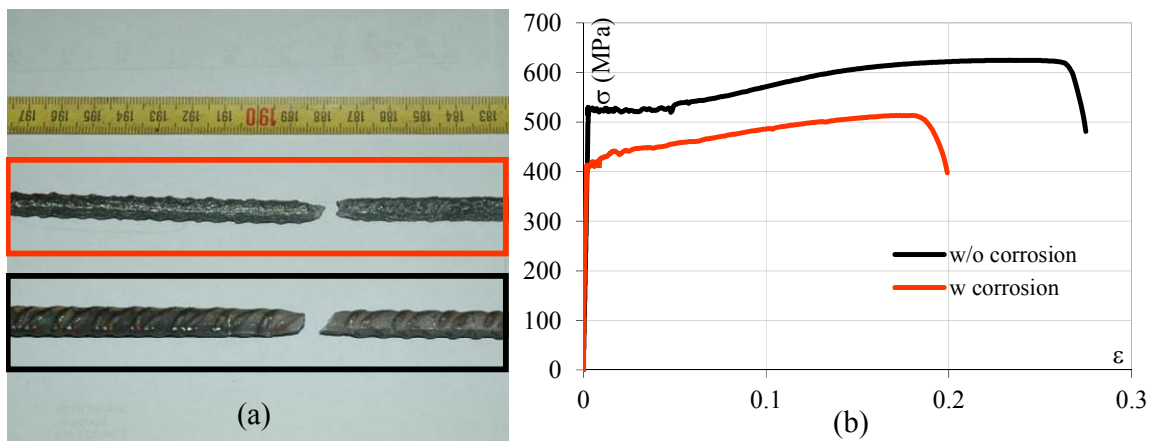


Fig. 5 (a) Close up view of a corroded and not corroded steel bar at the end of the tensile tests and (b) Typical results of tensile tests on corroded and not corroded steel bars

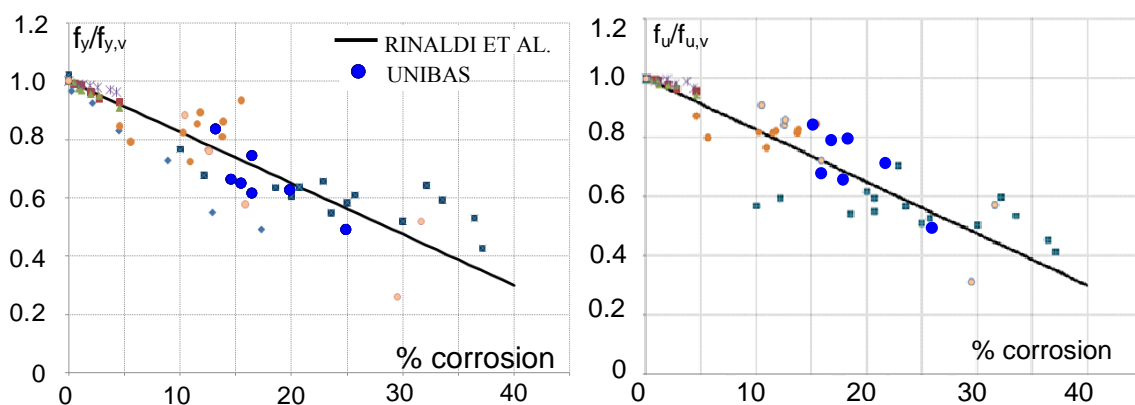


Fig. 6 Comparison between the experimental results of the tensile tests carried out at the UNIBAS Laboratory and the corrosion decay law proposed by Rinaldi *et al.* (2007)

In Fig. 6 the experimental results of the tensile tests carried out at the Laboratory of UNIBAS are compared to the analytical law of strength reduction due to corrosion, recently proposed by Rinaldi *et al.* (2007). The comparison is made in terms of yielding stress (f_y) and ultimate stress (f_u), normalized with respect to the same characteristics of the corresponding virgin sample ($f_{y,v}$ and $f_{u,v}$ respectively). Both stress ratios are reported as a function of the level of corrosion, expressed by the percentage of reduction of the bar diameter. As can be seen, the results of the experimental tests conducted in this study are in good accordance with the corrosion decay law proposed by Rinaldi *et al.* (2007), which also includes a relationship for the estimation of the ultimate ductility of corroded rebars. As a consequence, in the numerical analyses presented in this study, reference to the analytic law by Rinaldi *et al.* (2007) has been made, in order to estimate the mechanical properties of steel for different corrosion states.

3.4 Test configuration

Fig. 7 shows the test apparatus. It consists in a very stiff steel structure, simulating the bridge deck, driven by a double-acting servo-hydraulic dynamic actuator (connected by cylindrical joints to the reaction wall), which applies the horizontal seismic forces/displacements to the deck. A couple of pseudo-dynamic actuators (fixed at the ground and lined up to the pier) are used to reproduce the tributary weight of the deck, equal to 650 kN (corresponding to 5850 kN in the full-size prototype scale). The pseudo-dynamic actuators work under force control. The total force applied by the two pseudo-dynamic actuators is maintained constant during the tests. The dynamic actuator, instead, is driven under displacement control. In the cyclic tests, the input signal of the dynamic actuator is represented by a sinusoidal displacement-time history of increasing amplitude.

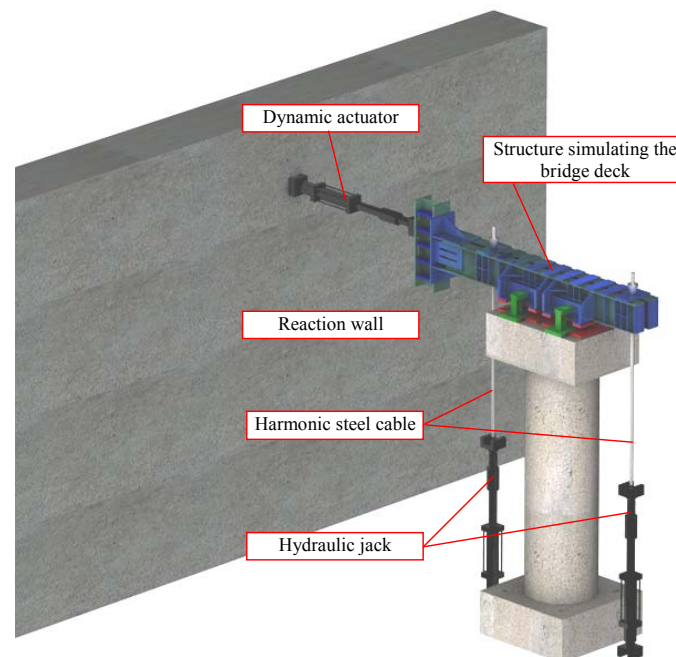


Fig. 7 3D view of the test apparatus for cyclic tests of pier-deck systems

The steel structure that simulate the deck has been designed to accommodate different types of connection between deck and pier cap, including: (1) rigid connections, realised by stiff Z-shaped steel sections and (2) semi-rigid connections, realised by traditional neoprene pads. The numerical simulation analyses described in this paper have been conducted assuming the deck rigidly connected to the pier cap by means of stiff Z-shaped steel sections. More detailed information on experimental models and test set-up can be found in Cardone *et al.* (2010).

4. Numerical simulation analyses of cyclic tests

4.1 Modeling assumptions

Fig. 8 shows the layout of the numerical model implemented in OpenSees (McKenna *et al.* 2000), to analyse the cyclic behaviour of the piers.

Particular care has been taken in reproducing the actual test set-up (see Fig. 7). The steel structure simulating the bridge deck has been modelled with a rigid assemblage of truss elements (see Fig. 8). The vertical actuators, through which the gravity load of the deck is applied, have been taken into account by means of two equivalent static forces. The effects of the horizontal actuator have been described by assigning a suitable cyclic displacement-time history function. Piers have been modelled with fibre elements with distributed plasticity. Rigid link elements have been adopted to model pier cap and foundation (see Fig. 8).

More in detail, piers have been modelled with nonlinear force-based (FB) fibre elements with distributed plasticity (available in OPENSees), in lieu of the displacement-based (DB) fibre elements. DB fibre elements use given displacement interpolation functions along the element. This requires the use of a proper mesh of the elements to get an accurate structural response, that implies computational efforts (Neuenhofer *et al.* 1997, 1998). FB fibre elements, on the contrary, use exact force interpolation functions. In that case, numerical integration errors are reduced by increasing the number of integration points instead of the number of elements (Neuenhofer *et al.* 1997, 1998).

In this study, therefore, piers have been modelled with one FB fibre element characterized by five Gauss-Lobatto integration points. The pier cross section has been divided into 1440 concrete fibres, distinguishing unconfined concrete (240 fibres) and confined concrete (1200 fibres). In addition, 96 steel fibres for the short piers and 40 steel fibres for the tall piers have been used to model the longitudinal reinforcement.

Four different stress-strain relationships have been used to describe the mechanical behaviour of (confined and cover) concrete and (corroded and not corroded) steel, and then assigned to the corresponding fibres of the pier model. The mechanical behaviour of unconfined concrete, in particular, has been modelled with the law by Kent-Scott-Park (1971). Reference to the model of Mander (1988) has been made for confined concrete. Finally, the constitutive model by Giuffrè-Menegotto-Pinto (1973) has been adopted for steel. All the aforesaid schematic stress-strain relationships have been calibrated based on the experimental results of the characterization tests carried out on the specimens collected during the construction of the piers.

The shear behaviour of the piers has been captured for short piers by introducing a nonlinear spring in series with the beam element. The shear resistance and stiffness of the pier have been computed based on the relationship proposed by Priestley *et al.* (2007).

Moreover, a zero-length element has been added to reproduce the pull-out effects of rebars. The

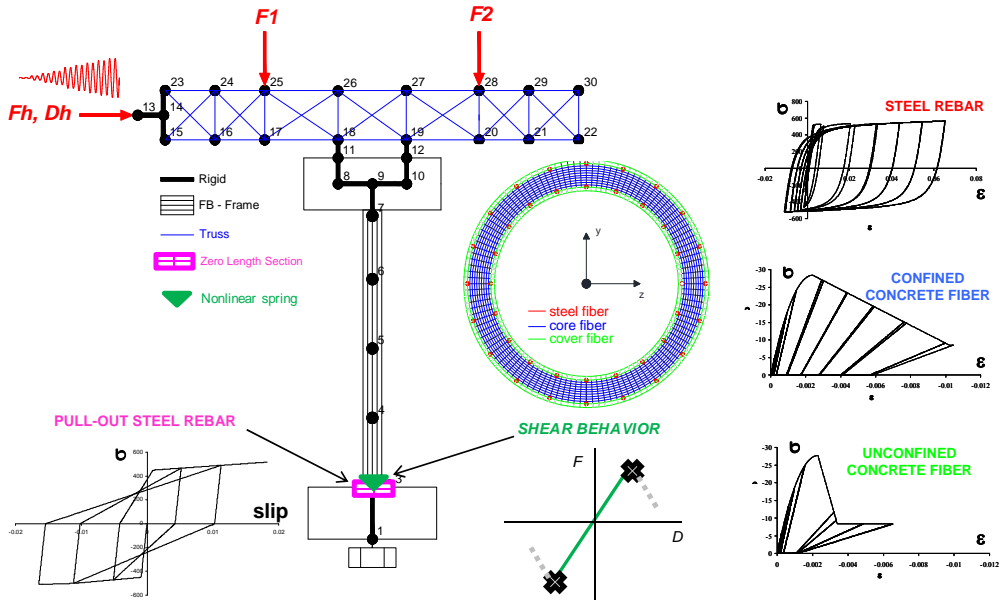


Fig. 8 Numerical modelling of RC piers using fibre elements: discretization of the transverse cross section and constitutive laws of materials

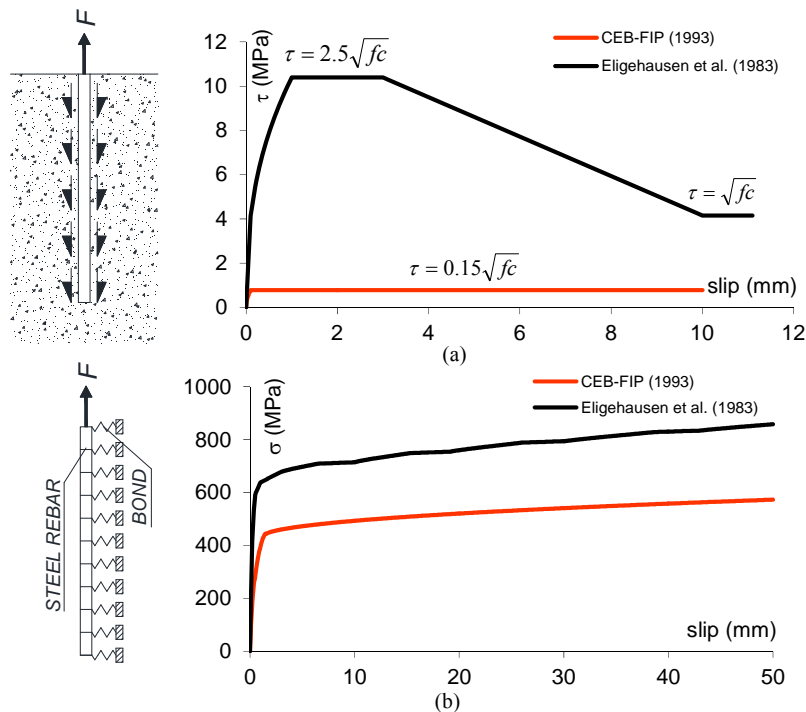


Fig. 9 (a) Modeling of pull-out effects and bond-slip relationships adopted for corroded and not corroded steel rebars (b) normal Stress vs. slip relationship obtained from SAP analyses

zero-length element has been placed at the base of the pier, close to foundation, as shown in Fig. 8. A number of pull-out tests have been numerically simulated with SAP2000-Nonlinear (2005), in order to define the normal stress vs. slip relationship of the steel bars for the zero-length element (see Fig. 9(b)). In the numerical simulations, the adherence between concrete and steel rebar has been modelled with a number of nonlinear shear springs (see Fig. 9(a)). The bond stress vs. slip relationships proposed by CEB-FIP (1993) and Eligehausen *et al.* (1983) have been adopted for corroded and not-corroded rebars, respectively. The concrete surrounding the steel bars inside the foundation has been deemed to be fully confined by the lateral pressure of the rest of the concrete foundation (Ranf *et al.* 2004).

4.2 Numerical results

Preliminary static pushover analysis have been carried out for each pier to evaluate the force displacement skeleton curve and the corresponding significant points such as: pier yielding, spalling of unconfined concrete and pier collapse. According to (Priestley *et al.* 2007), the following assumptions have been made:

- Pier yielding corresponds to the point of the force-displacement curve at which either the first steel fibre reaches the yield strain in tension or the first concrete fibre attains a compression strain of 0.002;
- Spalling of unconfined concrete occurs when the first unconfined concrete fibre reaches a compression strain of 0.004;
- Pier collapse is deemed to be achieved when one of the following conditions occurs: (1) the first steel rebar attains its ultimate tensile strain and (2) the first fibre of confined concrete reaches its residual compression stress.

Fig.10 shows the skeleton curves obtained from the numerical analyses for Tall (Fig.10(a)) and SHort piers (Fig.10(b)).

A yielding force and a maximum resistance of approximately 133 KN and 157 KN, respectively, were found for T/B/NC pier, which results just a little (less than 15%) greater than for the same pier with corroded rebars (T/B/C pier) (see Fig.10(a)). The ultimate displacement of the two piers results practically the same, equal to approximately 56 mm. This is because in both the cases, concrete crushing anticipates the steel failure, thus tapering the differences between the steel reinforcement of the two piers. The displacement ductility of the T/A/NC pier resulted significantly greater than for the T/B/NC pier (3.71 vs. 2.50), due to the higher ultimate strain of the Mix A concrete.

A yielding force and a maximum resistance of approximately 315 KN and 390 KN, respectively, were found for SH/B/NC pier, which results of 20% greater than for the same pier with corroded rebars (SH/B/C pier) (see Fig.10(b)). The ultimate displacement of the two piers results equal to approximately 23 mm. The displacement ductility of the SH/A/NC pier results slightly greater than for the SH/B/NC pier (2.46 vs.1.84), due to the higher ultimate strain of the Mix A concrete. The shear resistance little affects the nonlinear flexural behaviour of the SH/A/NC only.

Based on the pushover analyses, the sinusoidal displacement time history to be applied in the experimental cyclic tests have been defined (see Fig.10). As can be seen, the cyclic displacement amplitude will be progressively increased during each test. Three cycles will be performed for

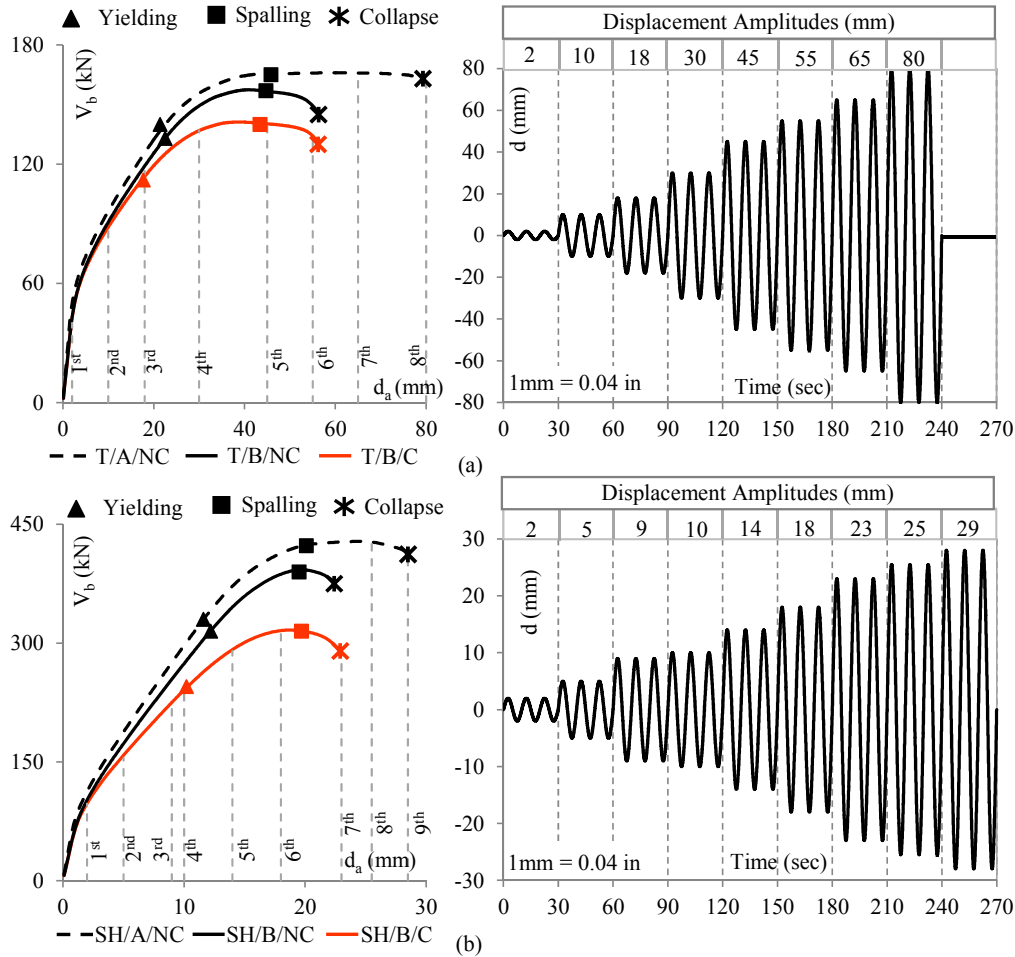


Fig. 10 (left) Skeleton curves obtained from the pushover analyses of (a) tall and (b) short piers and (right) actuator displacement time histories selected for the forthcoming experimental cyclic tests

each displacement amplitude. The first three displacement amplitudes correspond to the displacements associated to given fractions (approximately 10%, 60% and 100%) of the yielding force of the pier. The following displacement amplitudes correspond to the displacements associated to given fractions of the ultimate displacement ductility of the pier (see Fig. 10).

Once defined the input signals of the tests, the cyclic behaviour of the piers has been examined, considering different distributions and levels of corrosion, pull-out and overlap effects, as well as second-order ($P-\Delta$) effects.

Fig.11 shows the cyclic behaviour of T/B/C and SH/B/C piers. In both the cases an apparent pinching effect and a significant stiffness/strength degradation upon reloading is observed, while increasing the displacement amplitudes of the cycles.

Fig. 12 shows the hysteresis loops (base shear vs. actuator displacement) of the tall pier subjected to a constant axial force of 650 kN. Four different in-plan corrosion configurations (in the following referred to as C(0-360), C(90-270), C(180-360) and C(90-180), respectively) and

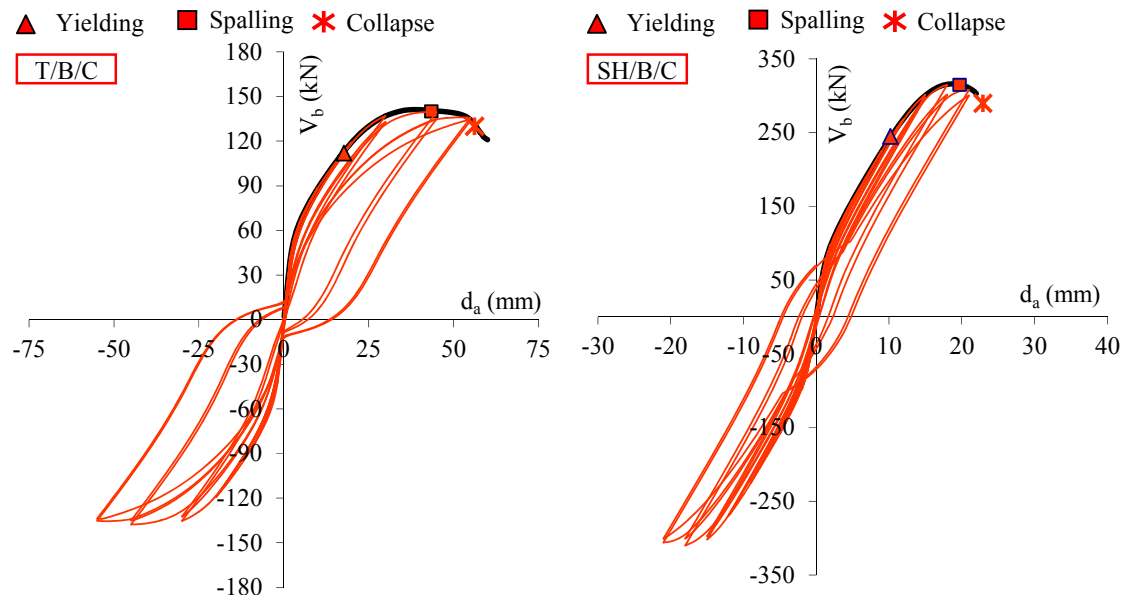


Fig. 11 Hysteresis loops (base shear vs. actuator displacement) of pier models T/B/C and SH/B/C

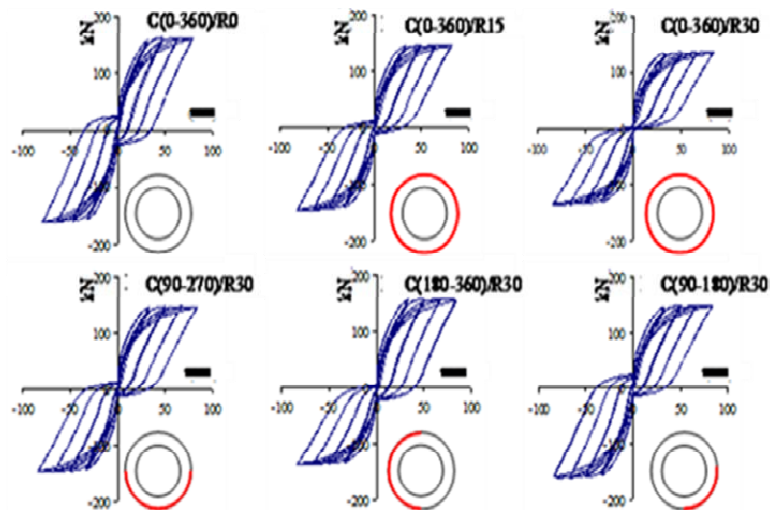


Fig. 12 Hysteresis loops (base shear vs. actuator displacement) of tall pier models characterized by different configurations and levels of corrosion

three different corrosion levels, corresponding to a reduction of the equivalent diameter of the steel rebars of the order of 0%, 15%, 30% (in the next referred to as $R0$, $R15$ and $R30$, respectively) have been considered. Corrosion was always limited to the longitudinal bars of the outer lateral

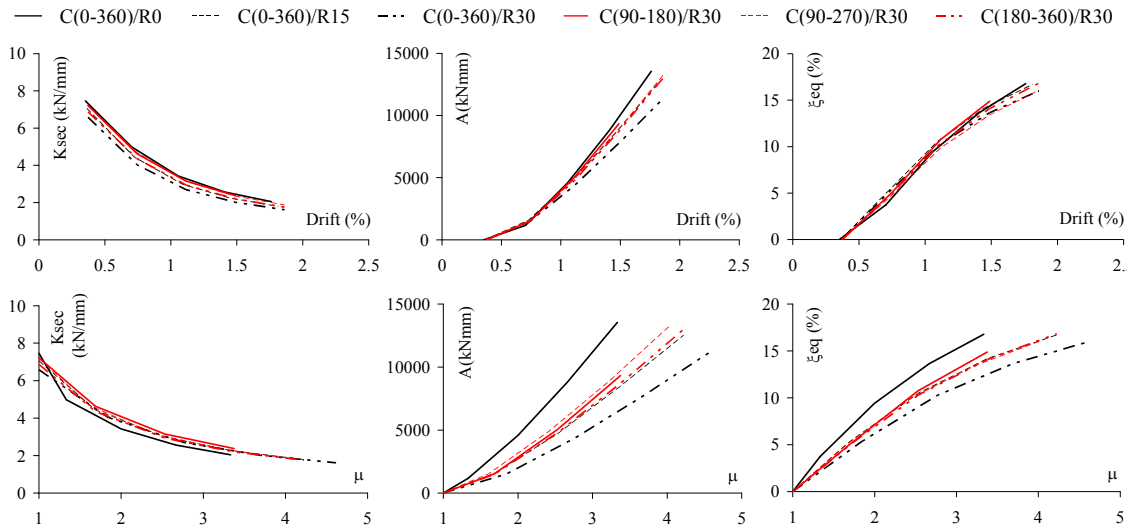


Fig. 13 Changes in secant stiffness (K), energy loss per cycle (A) and equivalent viscous damping (ξ_{eq}), as a function of pier drift and ductility ratio

surface of the pier. As can be seen in Fig. 12, the ultimate lateral strength of the pier reduces (approximately by 20%) while increasing the level of corrosion (from 0% to 30% in terms of reduction of equivalent diameter of steel rebar), mainly due to the decay in the mechanical characteristics of steel (see Fig. 5). On the other hand, the ultimate displacement of the pier increases (from 80 mm for C(0-360)/R0 to 84 mm for C(0-360)/R30) while the yield displacement decreases (from 19 mm for C(0-360)/R0 to 13 mm for C(0-360)/R30), due to the reduction of the longitudinal reinforcement ratio (from 0.6% to 0.46%) caused by higher levels of corrosion.

In Fig. 13 the mechanical behaviour of the six pier models is examined in terms of secant stiffness (K) at the maximum cyclic displacements, energy loss per cycle (A) and equivalent viscous damping (ξ_{eq}), evaluated with the Jacobsen's approach (1930). The results are reported as a function of both pier drift (i.e., top pier displacement divided by pier height) and ductility ratio (i.e., maximum cyclic displacement divided by a nominal yield displacement). The ultimate displacement of the pier has been assumed equal to the top pier displacement corresponding to the attainment of the residual stress in the first fibre of confined concrete. The nominal yield displacement has been derived from a bilinear idealization of the skeleton curve of the pier, according to the procedure described in Priestley *et al.* (2007). First, the elastic stiffness of the pier has been defined as the secant from the origin to the displacement corresponding to yielding of the first steel rebar. Next, the nominal yield displacement has been derived as intersection of the elastic stiffness with the force level corresponding to either a compression strain of 0.004 on the outer concrete fibres, or a tension of 0.015 on the outer steel rebar, whichever occurs first.

It is worth noting that ductility values greater than 3 have been found for C(0-360)/R0, in good accordance with the requirements of EC8 (CEN 2003), which recommend behaviour factors greater than 1.5 for hollow cylindrical piers with D_i/t ratio less than 8. The ductility of the piers with corroded rebars, results greater than 4 mainly due to the decrement of pier yield displacement.

Fig. 13 points out that the equivalent damping decreases while increasing the level of corrosion,

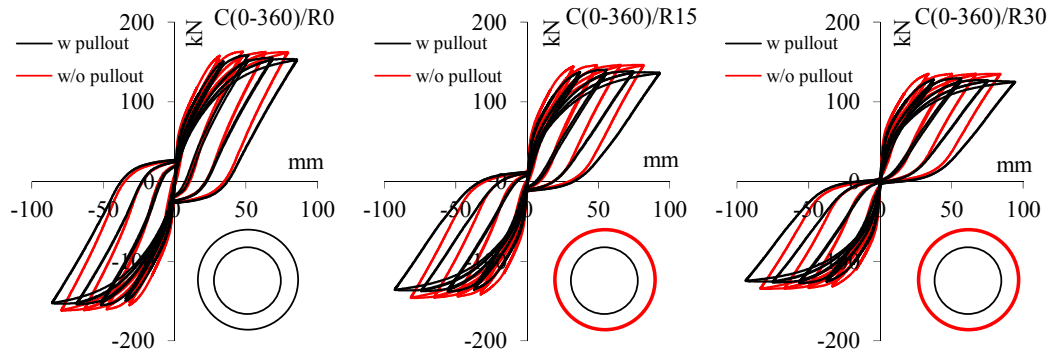


Fig. 14 Changes in the hysteresis loops of $C(0-360)/R0$, $C(0-360)/R15$ and $C(0-360)/R30$ piers considering pull-out and $P-\Delta$ effects

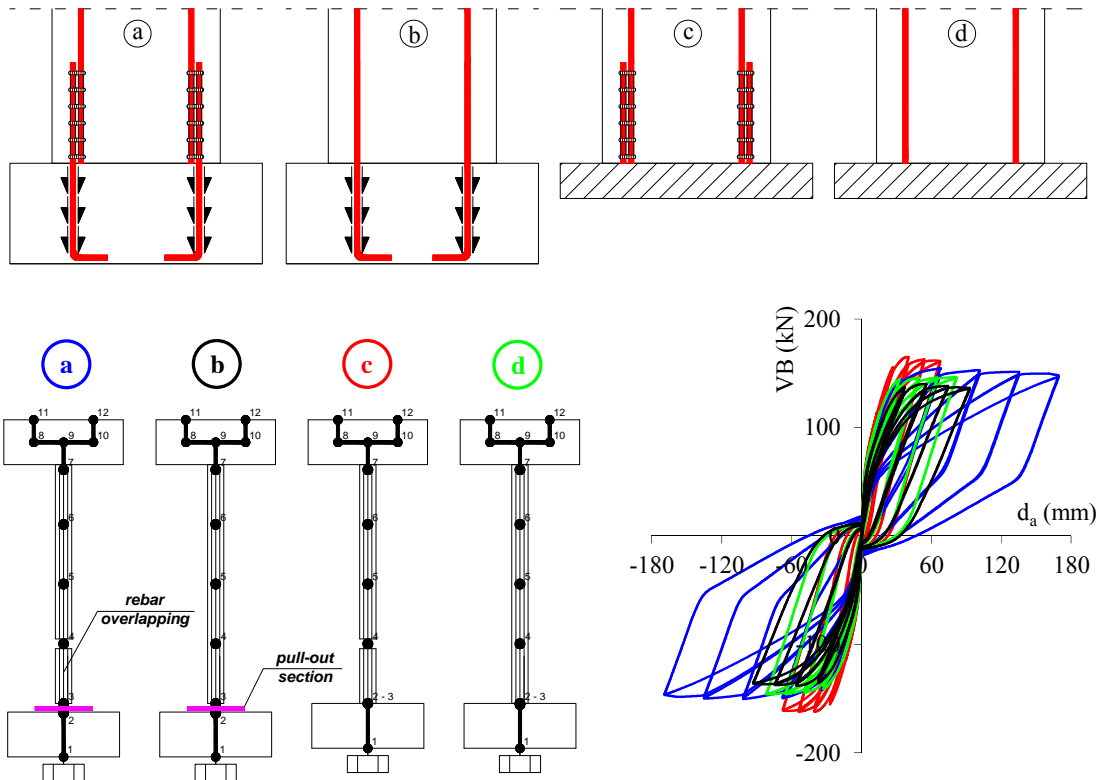


Fig. 15 Cyclic behaviour of T/A/NC considering different modelling assumptions: (1) w/ overlap and pull-out effects, (2) w/ pull-out effects and w/o overlap effects, (3) w/ overlap effects and w/o pull-out effects and (4) w/o overlap and pull-out effects

basically as a result of the reduction of the energy loss per cycle. For ductility values of the order of 2-3, for instance, the equivalent viscous damping reduces approximately by 25-20% (passing from 10-15% to 7.5-12%) for $C(0-360)/R15$ and by a further 10% (passing from 7.5-12% to 7-

11%) for $C(0-360)/R30$. The decrease of equivalent damping, however, is compensated by the increment of ductility. As a result, all the pier models exhibit similar equivalent damping values (of the order of 16%) at the limit pier drift ratio. Finally, the secant stiffness of the piers is little affected by corrosion (percent differences of the order of 10 %).

Fig. 14 shows the changes in the hysteresis loops of $C(0-360)/R0$, $C(0-360)/R15$ and $C(0-360)/R30$ considering pull-out and $P-\Delta$ effects. Basically, they determine a small decrease of the lateral strength and a little increase of the ultimate displacement of the pier. This clearly proves the good dimensioning of the anchorage of the steel rebars into the foundation. As expected, pull-out effects are more pronounced for the $C(0-360)/R30$ model, which undergoes a reduction of lateral strength of the order of 10 % and an increase of ultimate displacement of the order of 15%.

The influence of bar overlapping (in the region of plastic hinge, see Fig. 2) on the pier cyclic behaviour has been also investigated in the analyses. Four different modelling assumptions have been examined for $C(0-360)/R0$ pier. In the first model (see Fig. 15(a)) both bond-slip and overlap effects have been considered. The overlap effects have been then captured simply by doubling the number of rebars. A perfect bond (no slip) between overlapped bars has been assumed, due to an overlapping length of 0.6 m (23.62 in), which largely exceeds the minimum overlap length required by EC8 (CEN 2003). In the second model (see Fig. 15(b)), bar overlapping has been neglected while the pull-out effects of the rebars from the foundation have been taken into account. Third and fourth model (see Figs. 15(c) and (d)) are similar to the previous ones, except for pull-out effects which are always neglected. The fourth model (see Fig. 15(d)) represents the model typically used in common practice. On the other hand, the first model can be considered as the most accurate model.

In Fig. 15 the base shear vs. actuator displacement curves obtained from cyclic analysis of the aforesaid four models are compared. As can be noted, the influence of modelling assumptions is nothing but negligible. Considering pull-out effects (compare model *b* and *d*) a slight reduction (12%) of lateral strength and a small increase (15%) of ultimate displacement is found. Considering overlap effects (compare model *c* and *d*) an increase (20%) of lateral strength and a slight reduction (10%) of ultimate displacement is observed. Considering both pull-out and overlap effects (compare model *a* and *d*) leads to a significant increase of the ultimate displacement capacity of the pier (from approximately 80 mm to approximately 170 mm), essentially due to large slips of the corroded steel rebars into the foundation. The lateral strength, instead, remains practically the same (differences less than 10%), as overlap effects tend to counterbalance pull-out effects.

5. Future researches

The results of the numerical simulation analyses presented in this paper have been used to define important details of the forthcoming experimental tests. The cyclic (and pseudodynamic) tests will be performed at the Laboratory of Structures and Materials of the University of Basilicata at Potenza (Italy) in 2013. A comprehensive comparison between experimental results and numerical predictions will be carried out at the end of the experimental tests. Most likely, a model updating will follow. A substantial understanding of the phenomena involved in the experimental tests will be then possible, by examining the results of the updated numerical model.

6. Conclusions

A comprehensive experimental program of cyclic tests on 1:3-scale models of bridge piers is going to be carried out at the Laboratory of Structures and Materials of the University of Basilicata at Potenza (Italy). The testing models include eight RC single shaft piers with hollow circular cross section. Four piers have been realised using corroded steel rebars.

In this paper, the results of preliminary numerical simulation analyses have been presented, mainly with the scope of designing the forthcoming experimental program and evaluating the influence of corrosion of steel rebars on the cyclic behaviour of the piers. The effects due to pull-out of the steel rebars of the pier from foundation and bar overlapping in the zone of plastic hinge have also been investigated. The accuracy of the analyses performed is guaranteed by the use of fiber element and constitutive laws of materials derived from experimental tests on concrete and steel specimens.

As expected, the corrosion of steel rebars determines a significant reduction of the lateral strength, secant stiffness and energy loss per cycle of the piers. On the other hand, the equivalent viscous damping of the piers remains substantially unchanged, for the same pier drift. The results of the analyses have also shown that pull-out effects and overlap effects can significantly affect the cyclic behaviour of RC piers, especially in terms of ultimate displacement.

Acknowledgements

This work has been partially funded by the Italian Ministry for the University and the Research (MUR), within the SAGGI research project, led by Autostrade per l'Italia SpA. The authors are grateful to Domenico Nigro (University of Basilicata) for his valuable help in executing the accelerated corrosion process and the experimental characterization tests of materials.

References

- Auyeung, Y.B., Balaguru, P. and Chung, L. (2000), "Bond behavior of corroded reinforcement bars", *ACI Mater. J.*, **97**(2), 214–221.
- Bertolini, L., Elsener, B., Pedferri, P. and Polder, R.B. (2004), *Corrosion of steel in concrete: prevention, diagnosis, repair*, Wiley-VCH.
- Calvi, M.G., Pavese, A., Rasulo, A. and Bolognini, D. (2005), "Experimental and numerical studies on the seismic response of R.C. hollow bridge piers", *B. Earthq. Eng.*, **3**(3), 267–297.
- Cardone, D., Dolce, M., Pardi L., Perrone, G. and Sofia, S. (2010), "Pseudodynamic and cyclic tests on reduced-scale pier-deck sub-systems", *Proc. of the IABMAS*, Pennsylvania, USA.
- CEB. (1993), *CEB-FIP model code 1990 – Design Code*, Comité Euro – International du Béton, Thomas Telford, London.
- CEN, prEN1998-2. (2003), *EC8: Design provisions for earthquake resistance of structures. Part 2: Bridges*.
- Červenka, J. and Papanikolaou, V.K. (2008), "Three dimensional combined fracture-plastic material for concrete", *Int. J. Plasticity*, **24**(12), 2192–220.
- Choe, D., Gardoni, P., Rosowsky, V.D. and Haukaas, T. (2009), "Seismic fragility estimates for reinforced concrete bridges subject to corrosion", *Struct. Saf.*, **31**(4), 275–283.
- Computer and Structures, inc. (2005), *SAP2000 Advanced: Static and dynamic analysis finite element analysis of structures*, University Ave. Berkeley, CA.

- Delgado, P., Monteiro, A., Arêde, A., Vila Pouca, N., Delgado, R. and Costa, A. (2011), "Numerical simulations of RC hollow piers under horizontal cyclic loading", *J. Earthq. Eng.*, **15**(6), 833-849.
- Eligehausen, R., Popov, E.P. and Bertero, V.V. (1983), "Local bond stress-slip relationships of deformed bars under generalized excitations", *Report to the National Science Foundation, College of Engineering, University of California at Berkeley*, no. UCB/EERC – 83/23.
- Faria, R., Oliver, J. and Cervera, M. (1998), "A strain based plastic viscous damage model for massive concrete structures", *Int. J. Solids Struct.*, **35**(14), 1533–1558.
- Ghosh, J. and Padgett, J.E. (2012), "Impact of multiple component deterioration and exposure conditions on seismic vulnerability of concrete bridges", *Earthq. Struct.*, **3**(5), 649-673.
- Jacobsen, L.S. (1930), "Steady forced vibrations as influenced by damping", *Trans.-ASME*, **51**, 227.
- Kang, H.D., Willam, K., Shing, B. and Spacone, E. (2000), "Failure analysis of R/C columns, using a triaxial concrete model", *Comput. Struct.*, **77**(5), 423–440.
- Kent, D.C. and Park, R. (1971), "Flexural members with confined concrete", *Struct. Div.-ASCE*, 1971, **97**(7), 1969-1990.
- Kim, I., Lim, H., Jhun, G. and Kim, J. (2000), "Cyclic loading test of small scale bridge pier models without seismic detailing", *Proc. 12th WCEE*, Auckland, New Zealand.
- Kwon, M. and Spacone, E. (2000), "Three-dimensional finite element analyses of reinforced concrete columns", *Comput. Struct.*, **80**(2), 199–212.
- Liu, J. and Foster, S.J. (2000), "A three-dimensional finite element model for confined concrete structures", *Comput. Struct.*, **77**(5), 441–451.
- Mander, J.B., Priestley, M.J.N. and Park, R. (1988), "Theoretical stress-strain model for confined concrete", *J. Struct. Div.-ASCE*, **114**(8), 1804-1826.
- McKenna, F., Fenves, G.L. and Scott, M.H. (2000), "Open system for earthquake engineering simulation", <http://opensees.berkeley.edu>.
- Menegotto, M. and Pinto, P.E. (1973), "Method of analysis of cyclically loaded RC plane frames including changes in geometry and non-elastic behavior of elements under normal force and bending", *Preliminary Report, IABSE*, **13**, 15–22.
- Neuenhofer, A. and Filippou, F.C. (1997), "Evaluation of nonlinear frame finite-element models", *J. Struct. Eng.*, **123**(7), 958–966.
- Neuenhofer, A. and Filippou, F.C. (1998), "Geometrically nonlinear flexibility-based frame finite element", *J. Struct. Eng.*, **124**(6), 704-711.
- Papanikolaou, V.K. and Kappos, A.J. (2009a), "Numerical study of confinement effectiveness in solid and hollow reinforced concrete bridge piers: Methodology", *Comput. Struct.*, **87**(21-22), 1427–1439.
- Papanikolaou, V.K. and Kappos, A.J. (2009b), "Numerical study of confinement effectiveness in solid and hollow reinforced concrete bridge piers: Analysis results and discussion", *Comput. Struct.*, **87**(21-22), 1440–1450.
- Pinto, A.V., Molina, J. and Tsionis, G. (2003), "Cyclic tests on large-scale models of existing bridge piers with rectangular hollow cross-section", *Earthq. Eng. Struct. D.*, **32**(13), 1995–2012.
- Priestley, M.J.N., Calvi, G.M. and Kowalski, M. (2007), *Displacement based seismic design of structures*, IUSS Press, Pavia.
- Ranf, R.T. and Eberhard, M.O. (2004), "Development of 3-dimensional strain penetration analytical model in OpenSees", University of Washington, <http://www.ce.washington.edu>.
- Ranzo, G. and Priestley, M.J.N. (2001), *Seismic performance of circular hollow columns subjected to high shear*, The University of California, Report No. SSRP 2001/01.
- Rinaldi, Z., Valente, C. and Pardi, L. (2007), "A simplified methodology for the evaluation of the residual life of corroded elements", *Struct. Infrastruct. Eng.*, **4**(2), 139-152.
- Sadrnejad, S.A. and Labibzadeh, M. (2006), "A continuum/discontinuum micro plane damage model for concrete", *Int. J. Civil Eng.*, **4**(4), 296-313.
- Stewart, M.G. and Rosowsky, V.D. (1998), "Time-dependent reliability of deteriorating reinforced concrete bridge decks", *Struct. Saf.*, **20**(1), 91–109.
- Thoft-Christensen, P. (1998), "Assessment of the reliability pro-files for concrete bridges", *Eng. Struct.*,

- 20(11), 1004-1009.
- Whittaker, D., Park, R. and Carr, A.J. (1987), "Experimental tests on hollow circular concrete columns for use in offshore concrete platforms", *Proceedings, Pacific Conference on Earthquake Engineering, New Zealand*, **1**, 213-224.
- Yeh, Y.K., Mo, Y.L. and Yang, C.Y. (2001), "Seismic performance of hollow circular bridge piers", *ACI Struct. J.*, **98**(6), 862-871.
- Yeh, Y.K., Mo, Y.L. and Yang, C.Y. (2002), "Full-scale tests on rectangular hollow bridge piers", *Mater. Struct.*, **34**(246), 117-125.
- Zahn, F.A., Park, R. and Priestley, M.J.N. (1990), "Flexural strength and ductility of circular hollow reinforced concrete columns without confinement on inside face", *ACI Struct. J.*, **87**(2), 156-166.

CC